Cellular/Molecular

Syntaxin1A Lateral Diffusion Reveals Transient and Local SNARE Interactions

Claire Ribrault,[1] Jürgen Reingruber,[2] Maja Petković,[3,4] Thierry Galli,[4] Noam E. Ziv,[5] David Holcman,[2] and Antoine Triller[1]

[1]Biologie Cellulaire de la Synapse and [2]Theoretical Modeling of Cellular Physiology, Institut de Biologie de l'Ecole Normale Supérieure, Institut National de la Santé et de la Recherche Médicale Unité 1024 –CNRS 8197, F-75005 Paris, France, [3]Program in Development and Neurobiology, Institut Jacques Monod, CNRS, UMR 7592, Université Paris Diderot, Sorbonne Paris Cité, F-75205 Paris, France, [4]Institut National de la Santé et de la Recherche Médicale Équipe de Recherche Labellisée Unité 950, "Membrane Traffic in Neuronal and Epithelial Morphogenesis," F-75013 Paris, France, and [5]Department of Physiology and Biophysics and Rappaport Institute, Technion Faculty of Medicine, and Network Biology Research Laboratories, Haifa 32000, Israel

At the synapse, vesicles stably dock at the active zone. However, in cellular membranes, proteins undergo a diffusive motion. It is not known how the motion of membrane proteins involved in vesicle exocytosis is compatible with both vesicle docking and the dynamic remodeling of the plasma membrane imposed by cycles of exocytosis and endocytosis. To address this question, we studied the motion of the presynaptic membrane protein syntaxin1A at both the population and single-molecule levels in primary cultures of rat spinal cord neurons. Syntaxin1A was rapidly exchanged between synaptic and extrasynaptic regions. Changes in syntaxin1A mobility were associated with interactions related to the formation of the exocytotic complex. Finally, we propose a reaction-diffusion model reconciling the observed diffusive properties of syntaxin at the population level and at the molecular level. This work allows us to describe the diffusive behavior and kinetics of interactions between syntaxin1A and its partners that lead to its transient stabilization at the synapse.

Introduction

Synaptic vesicle exocytosis relies on the formation of the SNARE complex (Söllner et al., 1993; Jahn and Scheller, 2006), involving the plasma membrane proteins syntaxin1A and SNAP-25 and the vesicle-associated protein synaptobrevin2, and is further regulated by proteins forming the exocytotic complex (Rizo and Südhof, 2002). Synaptic release occurs in a context in which membranes have to be considered as two-dimensional fluids (Singer and Nicolson, 1972); proteins diffuse laterally within membranes and engage in transient interactions with their partners (Edidin et al., 1976; Saxton and Jacobson, 1997; Lippincott-Schwartz et al., 2001; Vereb et al., 2003). In the nervous system, membrane proteins such as postsynaptic neurotransmitter receptors and presynaptic potassium voltage-gated ion channels move in and out of the synaptic region by lateral diffusion within minutes (Choquet and Triller, 2003; Dahan et al., 2003; Gómez-Varela et al., 2010). Cytoplasmic proteins such as postsynaptic gephyrin and actin (Star et al., 2002; Hanus et al., 2006) and presynaptic Munc13 and bassoon (Kalla et al., 2006; Tsuriel et al., 2009) also diffuse between synaptic and extrasynaptic regions within the cytosol. Interestingly, the characteristics of these motions are related to the functional states of the synapse (Lévi et al., 2008; Bannai et al., 2009) and contribute to its adaptation to neuronal activity (Heine et al., 2008).

A specific feature of the presynaptic membrane is that it has to reconcile the stability of the docked vesicles with the ability to quickly reorganize during frequent cycles of exocytosis and endocytosis (Südhof, 2004). In particular, presynaptic membrane proteins involved in the formation of the stable docking complex are expected to disperse during exocytosis and subsequently to reorganize to reconstitute the functional membrane structure. Yet to date, the dynamics of presynaptic membrane proteins involved in vesicle docking and fusion remain largely unknown.

To address these issues, we have investigated the lateral diffusion of syntaxin1A, a SNARE protein at the core of this exocytotic complex (Wu et al., 1999). Here, we accessed in real time the diffusive dynamics of syntaxin1A both at the population level using fluorescence recovery after photobleaching (FRAP) and at the single (or close to) molecule level using single-particle tracking (SPT). We have shown that syntaxin1A was rapidly exchanged by lateral diffusion between synaptic and extrasynaptic regions, and that its motion was slower at synaptic regions than at extrasynaptic regions. In addition, the motion of syntaxin was modulated by interactions with its partners, which we identified as being related to the formation of the exocytotic complex. Fi-

Received Aug. 8, 2011; revised Sept. 19, 2011; accepted Sept. 28, 2011.

Author contributions: C.R., T.G., N.E.Z., D.H., and A.T. designed research; C.R., J.R., and M.P. performed research; C.R. and J.R. analyzed data; C.R. and A.T. wrote the paper.

This work was supported by Institut National de la Santé et de la Recherche Médicale, by an Agence Nationale de la Recherche grant (MorphoSynDif), and by a grant from the High Council for Scientific and Technological Cooperation between France and Israel. C.R. was a recipient of a fellowship from the Ministère de la Recherche et de la Technologie, France, and was supported by Association Française contre les Myopathies. D.H. was supported by Human Frontier Science Program and a European Research Council Starting Grant. M.P. was supported by a doctoral fellowship from Ecole des Neurosciences de Paris (Paris School of Neuroscience). The funders had no role in study design, data collection and analysis, decision to publish, or preparation of this manuscript. We acknowledge the assistance of Shlomo Tsuriel and Michal Stern.

The authors declare no competing financial interests.

Correspondence should be addressed to Antoine Triller, Biologie Cellulaire de la Synapse, Institut de Biologie de l'Ecole Normale Supérieure, Institut National de la Santé et de la Recherche Médicale Unité 1024, CNRS 8197, 46 rue d'Ulm, F-75005 Paris, France. E-mail: triller@biologie.ens.fr.

DOI:10.1523/JNEUROSCI.4065-11.2011

Copyright © 2011 the authors 0270-6474/11/3117590-13$15.00/0

nally, based on these experimental data, we proposed a reaction-diffusion model of the diffusive behavior of syntaxin, which allowed us to estimate different kinetic parameters associated with the interactions between syntaxin and its partners that ultimately lead to its transient stabilization at the synapse.

Materials and Methods

Cell culture and transfection

Primary cultures of rat spinal cord neurons were prepared from 14-d-old Sprague Dawley rat embryos of either sex as previously described (Charrier et al., 2006). The culture conditions were such that only interneurons (and not motoneurons) could grow. Mouse spinal cord neurons were prepared from 13-d-old mouse embryo, from the gephyrin-mRFP knock-in mice raised in the laboratory using the same protocol. Neurons were transfected at 8 d *in vitro* (DIV) using Lipofectamine 2000, according to the manufacturer's protocol, with 1.5 μg of DNA per coverslip. Cells were imaged 24 h after transfection.

Plasmids

The plasmid for expression of syntaxin1A fused to pHGFP was a gift from T. A. Ryan (Weill Cornell Medical College, New York, NY) and is described by Mitchell and Ryan (2004). The SNARE and TMR constructs were derived from this plasmid, and encoded Stx1A, SNARE motif-TMR-GFP [Sx1A-(1–28 + 183–288) + pHGFP] and Stx1A, TMR-GFP [Sx1A-(1–28 + 259–288) + pHGFP], respectively. Coding sequences of all constructs have been verified by sequencing using the stx1A rat sequence as reference. The plasmid for expression of the light chain of botulinum toxin E (BoNT/E) was a gift from T. Galli (Insitut Jacques Monod, Paris, France).

Immunofluorescence labeling of fixed cells

Immunocytochemistry was performed as described previously (Charrier et al., 2006). The primary antibodies used were mouse anti-syntaxin1A (monoclonal; Synaptic Systems), mouse anti-synapsin I (clone 3C5; Millipore), and rabbit anti-synapsin I (Millipore). Secondary antibodies were Cy3-conjugated goat anti-mouse (Cy3-conjugated goat anti-rabbit and FITC-conjugated goat anti-rabbit from Jackson ImmunoResearch).

Live imaging and active synapse labeling

The recording medium consisted of phenol red-free minimal essential medium supplemented with glucose (33 mM; Sigma-Aldrich) and HEPES (20 mM), glutamine (2 mM), Na-pyruvate (1 mM), and B27 (1×) from Invitrogen. Active presynaptic terminals were stained with FM4-64 (2 μM; Invitrogen) in the presence of KCl (40 mM) for 30 s to stimulate vesicle recycling.

Acid bath application

Acidic solution at pH 5.5 contained 150 mM NaCl and 15 mM MES (2-[*N*-morpholino]ethane sulfonic acid, pK 6.1) in water. This solution was applied for <1 min before replacing it with the standard recording medium.

Immunoprecipitation and Western blotting

PC12 cells were electroporated with stx::pHGFP as previously described (Martinez-Arca et al., 2000). Immunoprecipitation was performed from stx::pHGFP transfected and control nontransfected PC12 cells. Mouse GFP antibody (Roche), mouse syntaxin1 (HPC1) antibody, and mouse IgG were covalently linked to Dynabeads protein G (Invitrogen). Two milligrams of cell lysate at stringent dilution of 1 mg/ml was incubated with Immunobeads overnight. Bound material was separated by SDS-PAGE, followed by Western. Membrane was cut and revealed with syntaxin 1 HPC1 and SNAP-25 71.1 (Synaptic Systems) antibodies using LI-COR technology.

Fluorescence recovery after photobleaching

Experiments were conducted using a FRAP microscope system (FRAP L5D; Roper Scientific) controlled by MetaMorph (Molecular Devices). It consisted of an inverted microscope (Eclipse TE2000-E; Nikon) equipped with an autofocus system (Nikon), a DG-4 illumination system (Sutter Instrument), and appropriate filter sets (Semrock; Optoprim). Coverslips were mounted on a chamber containing the recording medium and observed with a 100× objective (Nikon). Chamber and objective were heated at 36°C.

Circular regions (diameter, 1 μm), either at extrasynaptic or synaptic sites (identified by FM4-64 staining; see above), were bleached by high-intensity 488 nm laser (ERROL) for 8 ms at 60 mW. Fluorescence intensity was reduced by 60% after bleaching (first image was taken within <50 ms). Fluorescence recovery was then monitored by time-lapse acquisitions with a CCD camera (QuantEM 512SC; Roper Scientific) at 0.5 Hz for 10 s, 0.2 Hz for the next 110 s, and 0.1 Hz for an additional 120 s. To analyze the fluorescence recovery, fluorescence intensity was normalized to the fluorescence before bleaching and corrected for ongoing photobleaching with the following: $F_{corrt} = (F_t/F_0)/(F_{nbt}/F_{nb0})$, where F_t is the fluorescence at time t, F_0 is the fluorescence before bleaching, F_{nbt} is the average fluorescence intensity of three nonbleached spots at time t, and F_{nb0} is the average fluorescence intensity of the same nonbleached spots before bleaching (Tsuriel et al., 2006). Data were then further normalized to the initial fluorescence after bleach F_i: $F_{norm}(t) = (F_{corr}(t) - F_{corr}(\text{bleach}))/(F_{corr}(\text{before bleach}) - F_{corr}(\text{bleach}))$.

Fits of FRAP recovery curves were made according to the following equation: $F_t = P_f[1 - \exp(-t/\tau_f)] + (1 - P_f)[1 - \exp(-t/\tau_s)]$, where P_f is the relative size of the fast pool (expressed as a fraction of 1), and τ_f and τ_s are the recovery time constants for the fast and slow pools, respectively. The leastSquaresFit function implemented in Python was used to calculate the best fits. Most of the full curves could not be properly fitted with a biexponential fit; therefore, the fit was performed on the first portion of the recovery, between 0 and 50 s. The optimization was not done under constraints, however, and fits that gave "nonrealistic" parameters ($P_f > 1$ or < 0, and $\tau_s > 1000$) were discarded. Between 15 and 30 FRAP curves were averaged for each condition or location.

Single-particle tracking

Quantum dot labeling for single-particle imaging. Quantum dots (QDs) emitting at 605 nm conjugated with goat $F(ab')_2$ anti-rabbit IgG (Invitrogen) were first coupled with a rabbit anti-GFP antibody (Synaptic Systems).

Single-particle imaging. Neurons were imaged in the recording medium at 37°C in an open chamber mounted onto a IX70 inverted microscope (Olympus) equipped with a 60× objective (NA 1.45; Olympus). Fluorescence was detected using an Hg+ lamp, appropriate filters (QD: D455/70×, HQ605/20m; FM4-64: D535/50×, E590lpv2; GFP: HQ500/20, HQ535/30m; Chroma Technology) and a CCD camera (Cascade 512BFT; Roper Scientific). QDs were recorded during 500 consecutive frames with an exposure time of 75 ms. Cells were imaged for ~30–40 min after labeling.

Tracking and analysis. Single QDs were identified by their blinking (Dahan et al., 2003). Synaptic stain images were filtered using a multidimensional image analysis interface running in MetaMorph (Racine et al., 2007). QD location (synaptic or extrasynaptic) was identified by comparison with the filtered FM4-64 image (Dahan et al., 2003). Tracking was performed with homemade software (MATLAB; Mathworks). The center of the spot fluorescence was determined by Gaussian fit. Spatial resolution was ~10–20 nm. The spots in a given frame were associated with the most likely of the trajectories estimated on previous frames of the image sequence assuming free Brownian diffusion. For QDs, only trajectories with at least 15 consecutive frames were considered. For each condition, at least 80 trajectories were obtained. The mean square displacement (MSD) was calculated using $\text{MSD}(ndt) = (N-n)^{-1}\sum_{i=1}^{i=N-n}((x_{i+n}-x_i)^2 + ((y_{i+n}-y_i)^2)$, where x_i and y_i are the coordinates of an object on frame i, N is the total number of steps in the trajectory, dt is the time interval during two successive frames, and ndt is the time interval over which displacement is averaged. The diffusion coefficient D was calculated by fitting the first two to five points of MSD plot versus time with the equation $\text{MSD}(t) = 4D_{2-5}t + 4\sigma_x^2$; with σ_x the spot localization accuracy in one direction [references in the study by Ehrensperger (2007)]. Trajectories with $D < 10^4$ μm^2/s for QDs were classified as immobile. The size of the average confinement area was calculated by fitting the average MSD plot with the equation proposed by Kusumi et al. (1993) [references in the study by Ehrensperger (2007)]. A pause event was identified by a

portion of the trajectory where the instantaneous diffusion coefficient (calculated over 10 frames) was $<5 \times 10^{-2}$ $\mu m^2/s$. Only pause events longer than 12 frames (~1 s) were considered. Dwell time was calculated as in the study by Charrier et al. (2006), except that it was not averaged for each recording, but all the individual passages at synapses were considered.

Treatment with BAPTA-AM

BAPTA-AM was used at final concentration of 30 μM, in the medium used for live imaging. Stock solution was diluted in DMSO, so control measurements were performed with an equal volume of DMSO. Cells were incubated with BAPTA-AM for ~1 h including the labeling procedure. Imaging was done for an extra 30 min in the presence of BAPTA-AM.

Statistical analysis

Each set of experiments was performed on four to seven different neuron cultures. Data from different cultures were pooled, since intraculture variability was greater than interculture variability. Two-tailed Student's *t* tests were used, except for the non-normal distributions where Kolmogorov–Smirnov (KS) or Wilcoxon's tests were used, as indicated in the text.

Model of syntaxin diffusive behavior and fitting of FRAP recovery

The synaptic region was represented as a planar circular active zone 0.3 μm in radius, surrounded by a perisynaptic region that extends to a radius of 0.5 μm. The extrasynaptic region begins after the synaptic region and extends to a radius of 4 μm. The synaptic and extrasynaptic regions were connected by a transition region of width 0.2 μm, and the values of a parameter X in this region were interpolated from its synaptic and extrasynaptic values X_S and X_{ES} using the following transition function $Tr(r)$:

$$X(r) = X_S - (X_S - X_{ES})Tr(r)$$
$$Tr(r) = \frac{1}{2}\left(1 + \mathrm{Tanh}\left(\frac{2\left(r - \left(r_S + \frac{w}{2}\right)\right)}{w}\right)\right),$$

where r_S is the synaptic radius. This transition region may reflect a gradual change in the density of obstacles and interacting molecules from the synaptic to the extrasynaptic region. The radius of the extrasynaptic region was chosen such that it is sufficiently large to avoid strong depletion after bleaching. The cylindrical geometry of the axon was neglected since the synaptic diameter of the order of 0.6 μm is small compared with the axon circumference (of the order of 3 μm for an axonal radius of 0.5 μm) and diffusion in the extrasynaptic region is fast.

A Gaussian distribution was used to fit the experimental bleaching profile, which was ~1 μm in diameter (diameter at 50% fluorescence intensity). The recovery was measured in a circular spot of radius of 0.5 μm.

Modeling the molecular dynamics

As described in the main text, the diffusive behavior of syntaxin is modeled as resulting from free diffusion and binding reactions, according to the following equations:

$$\begin{array}{c} \overset{k_{01}}{S_0 + M_1 = S_1} \\ \overset{k_{10}}{\underset{k_{12}}{\quad}} \quad (*), \\ S_1 + M_2 = S_2 \\ \underset{k_{21}}{\quad} \end{array}$$

where S_0 is the free syntaxin molecule undergoing Brownian motion, S_1 is the first bound (immobilized) state, S_2 is the second bound (immobilized) state, M_1 and M_2 are abundant binding partners, and k_{10}, k_{12}, and k_{01}, k_{21}, the forward and backward binding rate constants. These parameters may differ in the synaptic and extrasynaptic regions.

Parameter estimation from SPT data. The diffusion coefficients were estimated from the SPT data (median of the distribution), as described above. The backward binding rates of the first reaction correspond to the inverse of the mean duration of binding (Schuss, 1980) and were therefore estimated from the duration of short pause events observed in SPT. The backward binding rates of the second reaction could not be estimated from SPT data since the duration of the long pauses could not be measured, so they remained free parameters in the model and were estimated from the fitting of FRAP experimental curves. The forward binding rates of both reactions could in principle be estimated from the frequency of pause events; however, a quantitative and precise estimation of these frequencies was hindered by technical limitations. The forward binding rates therefore also remained free parameters and were estimated from the fitting of FRAP experimental curves.

Fitting of the FRAP data. To fit the FRAP data, the following system of reaction-diffusion equations associated with the reactions described above (*) was numerically simulated as follows:

$$\frac{\partial}{\partial t} C_0(r,t) = \frac{1}{r}\frac{\partial}{\partial r}\left(rD(r)\frac{\partial}{\partial r}C_0(r,t)\right) - k_{01}(r)C_0(r,t) + k_{10}C_1(r,t)$$
$$\frac{\partial}{\partial t} C_1(r,t) = -(k_{10}(r) + k_{12}(r))C_1(r,t) + k_{01}(r)C_0(r,t) + k_{21}(r)C_2(r,t)$$
$$\frac{\partial}{\partial t} C_2(r,t) = -k_{21}(r)C_2(r,t) + k_{12}(r)C_1(r,t),$$

where, in polar coordinates, $C_0(r,t)$, $C_1(r,t)$, and $C_2(r,t)$ are the concentrations of free syntaxin (S_0), syntaxin in bound state S_1 and in bound state S_2, respectively. At steady state, the diffusional flux is zero and the steady state concentration C_0 of unbound syntaxin is independent of r. The steady-state concentrations of bound syntaxin C_1 and C_2 are as follows:

$$C_1(r) = \frac{k_{01}(r)}{k_{10}(r)}C_0$$
$$C_2(r) = \frac{k_{12}(r)}{k_{21}(r)}C_1(r) = \frac{k_{12}(r)k_{01}(r)}{k_{21}(r)k_{10}(r)}C_0,$$

and the total syntaxin concentration is as follows:

$$C = C_0 + C_1(r) + C_2(r) = C_0\left(1 + \frac{k_{01}(r)}{k_{10}(r)} + \frac{k_{12}(r)k_{01}(r)}{k_{21}(r)k_{10}(r)}\right).$$

Extrasynaptic parameters ($k_{01}{}^E$, $k_{12}{}^E$, and $k_{21}{}^E$) were obtained by fitting the experimental extrasynaptic FRAP curves. Experimental synaptic curves, which depend both on the dynamics of syntaxin at the active zone and at the surrounding extrasynaptic region, were fitted using the fitted values of the extrasynaptic parameters, allowing estimation of the synaptic parameters ($k_{01}{}^S$, $k_{12}{}^S$, and $k_{21}{}^S$).

Results

Syntaxin::GFP is regularly distributed along the axonal plasma membrane

Rat spinal cord neurons were transfected after 8 DIV with syntaxin1A fused to the pHluorin sequence at its extracellular C terminus (stx::pHGFP) (Mitchell and Ryan, 2004). pHluorin is a GFP variant that is not fluorescent at pH <6 when excited with blue light (Sankaranarayanan et al., 2000). All experiments described were performed at 9 DIV, a stage at which most spinal cord synapses are mature (Dumoulin et al., 2000). Stx::pHGFP was localized in the plasma membrane of transfected neurons: bath application of an acidic solution, pH 5.5, resulted in a total loss of pHluorin fluorescence that was reversible at physiological pH (Mitchell and Ryan, 2004), indicating that the pHluorin was exposed to the extracellular medium, and therefore that stx::pHGFP was entirely localized in the plasma membrane (Fig. 1*A*). Stx::pHGFP was present both in dendrites and axons, as shown by immunostaining of transfected cells for MAP2 and Tau, respectively (data not shown). In live neurons, axons contained active presynaptic boutons, identified by their ability to uptake the FM4-64 dye under KCl depolarization (Fig. 1*B*). In

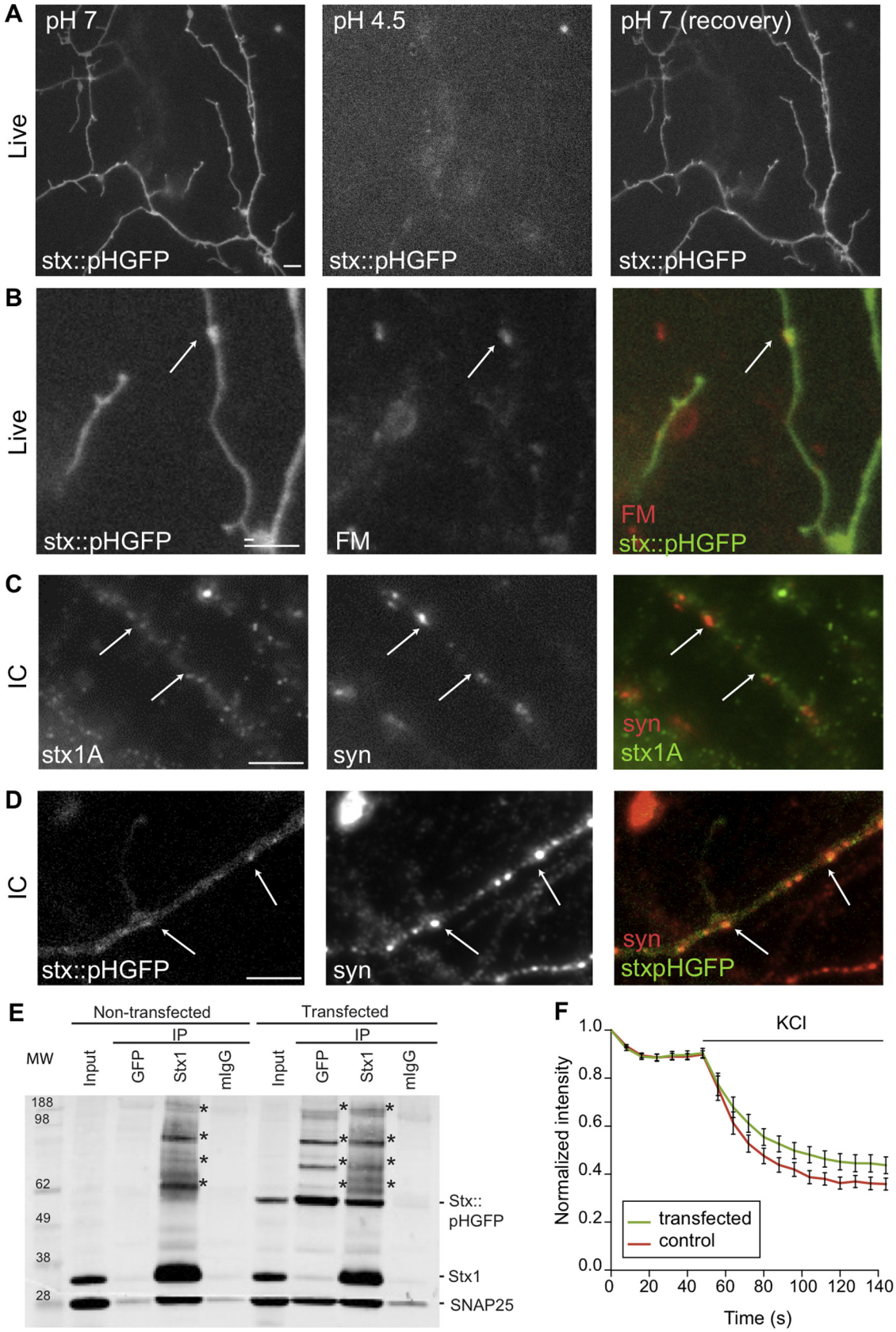

Figure 1. Expression of stx::pHGFP in spinal cord neurons. ***A***, ***B***, Live imaging of cultured spinal cord neurons (9 DIV) transfected with stx::pHGFP. ***A***, Surface stx::pHGFP fluorescence was quenched by bath application of media at pH 4.5. ***B***, Active synapses (arrows) were labeled with FM4-64 (FM4-64, red; stxGFP, green). ***C***, Syntaxin-1A (stx1A) (green) and synapsin (syn) (red) IF labeling in nontransfected neurons (9 DIV). The arrows show patches of stx1A colocalizing with synapsin. ***D***, Synapsin (Syn) (red) IF labeling in neurons transfected with stx::pHGFP (stxGFP;green). The arrows show patches of stx::pHGFP colocalizing with synapsin. Scale bar, 10 μm. ***E***, Coimmunoprecipitation of SNAP-25 with stx::pHGFP and syntaxin1 in transfected and nontransfected PC12 cells. Starting material (input) and eluate from Immunobeads (IP) coupled to syntaxin1 (stx1), GFP, and control mouse IgG (mIgG) were analyzed by Western blotting with syntaxin1 (*Figure legend continues*.)

addition, they could be distinguished from dendrites since they were thinner (compared with dendrites) and contained varicosities corresponding to synapses. In the following, we will focus only on axonal syntaxin1A. In the axons of live neurons, stx::pHGFP was regularly distributed (Fig. 1), with a slightly higher fluorescence intensity at synapses (syn/extrasyn, 1.2 ± 0.02; mean ± SEM). In live cells, the distribution of endogenous syntaxin1A could not be compared with that of stx::pHGFP with optical methods because immunostaining of endogenous syntaxin1A requires access to the intracellular domain of the protein (no antibody against the 6 aa extracellular domain is available). After fixation, permeabilization, and immunostaining, the distribution of endogenous syntaxin1A was even and patchy, in agreement with published data (Garcia et al., 1995; Hagiwara et al., 2005), and was comparable with that of stx::pHGFP (Fig. 1*C*,*D*). Stx::pHGFP was engaged in molecular interactions similar to endogenous syntaxin since stx::pHGFP coimmunoprecipitated with its SNARE partner SNAP-25, in an amount at least equal to those obtained for endogenous syntaxin (Fig. 1*E*). Finally, stx::pHGFP overexpression hardly affected exocytosis: FM4-64 unloading rate on application of KCl was only slightly lower in transfected neurons than in nontransfected neurons (Fig. 1*F*), which is consistent with previous studies in hippocampal neurons (Mitchell and Ryan, 2005). Overall, although the functionality of stx::pHGFP could not be definitely assessed, these data show a high similarity between the distribution and interactions of stx::pHGFP and those of the endogenous protein, and a minor effect of overexpression on exocytosis.

stx::pHGFP exchange dynamics within the plasma membrane is hindered at synapses

We compared the global dynamic behavior of stx::pHGFP at synaptic and extrasynaptic regions, by using FRAP. We bleached circular areas of ~1 μm diameter (diameter at 50% fluorescence intensity), at synaptic and extrasynaptic sites. The bleached area was therefore larger than the synaptic region (~400 nm in diameter as estimated from electron microscopy on cultured mouse spinal cord neurons; data not shown), which means that the bleached regions at synaptic sites contained both synaptic and extrasynaptic membrane. Bleaching regions of the size of the synapse was not possible because the size of the bleached spot is limited to a few hundred nanometers by diffraction of the laser beam and because for too small bleached areas recovery rates were faster and not accurately and reliably measurable. After the bleach, fluorescence was reduced to ~40% of its initial value and gradually recovered to reach a plateau (Fig. 2*A*,*B*). At any given time, the normalized recovery was smaller at synapses than at extrasynaptic sites: 51% at synapses versus 66% at extrasynaptic regions after 6 s ($p < 10^{-4}$), 68 versus 83% after 28 s ($p < 10^{-4}$), and 84 versus 94% after 150 s (i.e., at the plateau) ($p = 0.02$). A biexponential fit, which could be properly performed for most of the recovery profiles, was used to estimate three parameters (see Materials and Methods): a short characteristic time τ_f (fast), a long characteristic time τ_s (slow), and a fraction P_f that reflects the prevalence of the short characteristic time. τ_f was 4.2 versus 2.3 s at synapses and at extrasynaptic regions, respectively ($p = 0.009$), τ_s was 187 versus 126 s ($p = 0.17$), and P_f was 55 versus 66% ($p = 0.009$). In summary, the fluorescence recovery was slower at synaptic than at extrasynaptic regions both at short (seconds) and long (minutes) timescales.

Individual trajectories of stx::pHGFP exhibit different characteristics at synaptic and extrasynaptic regions

FRAP only gives bulk estimates of the mobility of proteins. To characterize the mobility of individual stx::pHGFP molecules, we used SPT, which allows tracking of individual trajectories with 15–20 nm resolution (Dahan et al., 2003). Stx::pHGFP molecules were labeled with QDs precoupled to anti-GFP antibodies (see Materials and Methods), and their motion was followed for 37.5 s at 13 Hz. Trajectories were then analyzed according to their localization, synaptic or extrasynaptic. Various diffusive behaviors were observed, ranging from Brownian motion within large areas (Fig. 3*Ai*), to confined diffusion (Fig. 3*Aii*), and "pauses" (Fig. 3*Aiii*). The analysis of the trajectories was based on the computation of the MSD of each particle as a function of time (Fig. 3*B*) (see Materials and Methods). First, the effective diffusion coefficient D (hereafter simply referred to as "diffusion coefficient") was obtained from the initial slope of the MSD, which is equal to $4D$ for a two-dimensional planar motion. Both at synapses and extrasynaptic regions, individual diffusion coefficients ranged from 10^{-4} to 1 $\mu m^2/s$ (10^{-4} $\mu m^2/s$ was taken as the limit of resolution). On average, the diffusion coefficient was smaller at synapses than at extrasynaptic regions (Fig. 3*B*). More specifically, the cumulative frequency distribution of diffusion coefficients at synapses was significantly shifted toward smaller diffusion coefficients compared with extrasynaptic regions (0.07 vs 0.20 $\mu m^2/s$, respectively, as median values; KS test, $p = 2 \times 10^{-16}$) (Fig. 3*C*). Second, trajectories were described as resulting from Brownian motion when the MSD was a linear function of time, and as resulting from confined motion when the MSD curve saturated (see Materials and Methods). A higher proportion of trajectories was confined at synapses that at extrasynaptic sites (72.61 ± 3.83% vs 48.66 ± 4.55%, respectively; mean ± SEM; $p = 0.004$). The characteristic length of confinement, which describes the diameter of the region in which the trajectory is confined, was smaller at synapses than at extrasynaptic regions (338 vs 662 nm; median values; $p < 10^{-12}$, KS test) (Fig. 3*D*). Third, some trajectories displayed periods during which the QD-labeled stx::pHGFP underwent a strong and rapid decrease in the instantaneous diffusion coefficient (about 2 orders of magnitude) (see Materials and Methods). These trajectories (or portions of trajectories) were called "pauses." During pauses, the diffusion coefficient was notably small (Fig. 3*B*,*C*) (median, 2.3×10^{-4} $\mu m^2/s$). The explored area was 128 nm wide (median) (Fig. 3*D*). These pauses lasted from a few seconds to a few minutes (a few 5 min recordings were made to show that pauses could last up to a few minutes). During the 37.5 s recordings, we distinguished between trajectories where the QDs paused throughout the recording session ("long pauses"), those for which only one end of the pause could be observed ("truncated pauses"), and those for which both ends were observed ("short pauses"). The frequency of these events at synaptic and extrasynaptic sites was obtained by dividing their number at each location by the residence time of QD-labeled stx::pHGFP in synaptic and extrasynaptic regions, respectively (see Materials and Methods). Pause events were more frequent at synapses than at extrasynaptic regions (0.007 vs 3×10^{-4} s^{-1}, $p = 0.01$, for long pauses; 3×10^{-3} vs 6×10^{-4} s^{-1}, $p = 0.09$, for truncated pauses; and $2 \times$

←

(*Figure legend continued.*) antibody, revealing monomeric syntaxin1 and undissociated complexes (*), and SNAP-25 antibody, showing coimmunoprecipitation of SNAP-25 with endogenous syntaxin1 (lane 2) or stx::pHGFP (lane 7). MW, Molecular weight (in kilodaltons). ***F***, Simultaneous destaining of FM4-64 from synaptic vesicles of nontransfected control cells (red) and stx::pHGFP expressing cells (green) in the same culture dishes, during 40 mM KCl application. The destaining rate is slightly lower in transfected cells than in nontransfected cells.

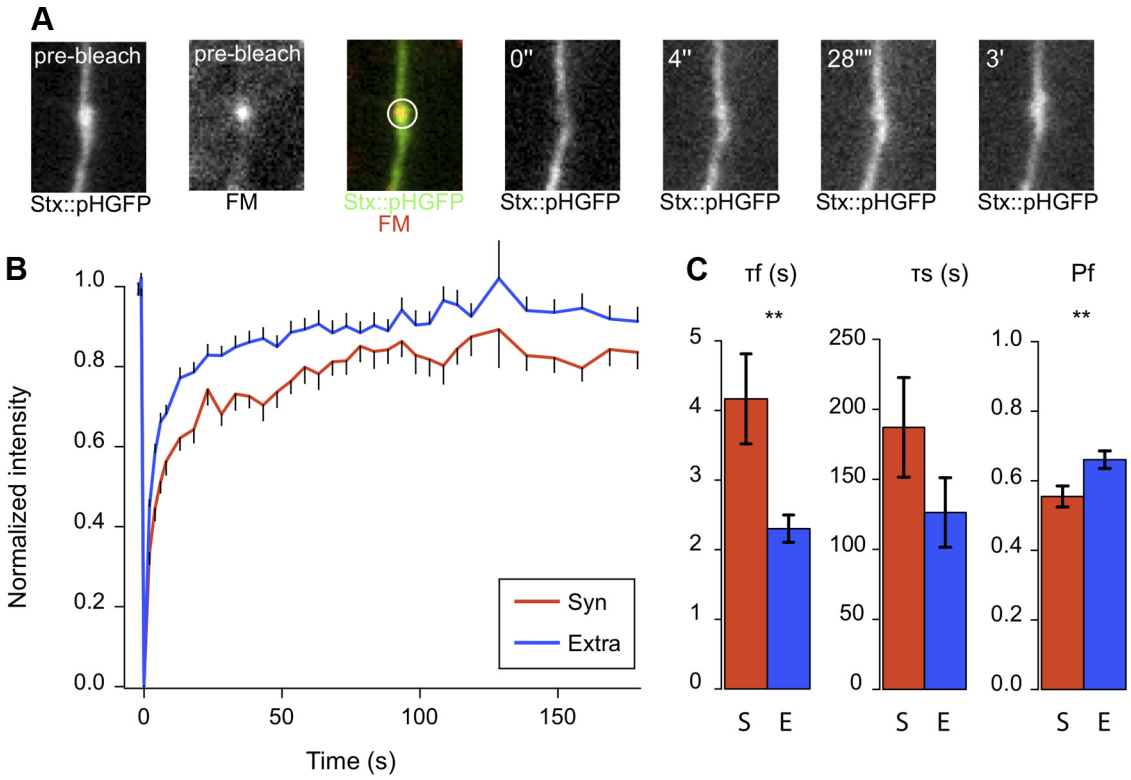

Figure 2. Slower rates of fluorescence recovery after photobleaching of stx::pHGFP at synaptic and extrasynaptic regions. ***A***, Examples of images recorded during a FRAP experiment. Images of stx::pHGFP and synapses labeled with FM4-64 (FM) were taken before the bleaching ("prebleach"). The bleached area is indicated by a white circle on the corresponding overlay. Images from the time lapse recording following the bleaching are shown at times 0 s, 4 s, 28 s, and 3 min. ***B***, Averaged normalized fluorescence recovery of stx::pHGFP (mean ± SEM) versus time at synaptic (red) and extrasynaptic (blue) regions. ***C***, Parameters from the biexponential fit of the experimental curves (see Materials and Methods): short characteristic time τ_f, long characteristic time τ_s, and fast fraction P_f (mean ± SEM), for synaptic (red) and extrasynaptic (blue) regions. Two-tailed *t* test, $^{**}p < 0.01$.

10^{-3} vs 1×10^{-3} s^{-1}, $p = 0.7$, for short pauses) (Fig. 3*E*). The median duration of the short pauses was 4.5 s. Therefore, the short pauses are not likely to correspond to the tail of the distribution of the long pauses, but correspond to a different population. Finally, some of the pause trajectories displayed a specific pattern, in which the particle switched between adjacent subdomains (Fig. 3*Fi*). To analyze these trajectories, the positions of the particle were first classified into subdomains on the basis of the distance between the different positions (Fig. 3*Fii*), using a Gaussian mixture analysis (see Materials and Methods). Then, the distance of the particle to the center of mass of each subdomain was measured as a function of time (Fig. 3*Fiii*). In the example presented here, the particle switched between two domains ~70 nm apart, spending a few seconds in the first subdomain before moving to the other one. This behavior could correspond to consecutive pauses at adjacent locations.

In summary, SPT revealed a large heterogeneity of diffusive behaviors. The slower, more confined diffusion and the more frequent pauses at synapses were consistent with the slower recovery kinetics observed in FRAP experiments at synapses compared with extrasynaptic regions.

Intracellular interactions affect the trajectories of stx::pHGFP

We then asked how intracellular interactions between syntaxin and its partners (Wu et al., 1999; Rizo and Rosenmund, 2008) could influence the characteristics of its motion. Syntaxin1A consists of three main domains (Misura et al., 2000): a C-terminal transmembrane domain, a SNARE domain (involved in the formation of the SNARE complex), and the N-terminal Habc domain, involved in interactions with Munc proteins (Südhof and Rothman, 2009). We characterized the motion of two truncated constructs of stx::pHGFP (Fig. 4*A*): snareGFP (hereafter called "SNARE"), where the Habc domain was deleted (amino acids 1–28, 183–288), and tmrGFP ("TMR"), where both the Habc and the SNARE domains were deleted, consisting only of the transmembrane region and a small N-terminal domain (amino acids 1–28, 259–288). In SPT experiments, for each construct taken independently, the motion remained different between synaptic and extrasynaptic regions (Fig. 4*A–D*): as for the full-length stx::pHGFP ("FL"), at synapses compared with extrasynaptic regions, trajectories had smaller diffusion coefficients (Fig. 4*B*,*C*) ($p = 2 \times 10^{-16}$, KS test), they were more frequently confined (SNARE: 74.84 vs 43.90%, $p = 2 \times 10^{-5}$; TMR: 69.11 vs 45.21%, $p = 0.02$), the characteristic length of confinement was smaller, and pauses were more frequent (Fig. 4*D*). However, the dynamic behaviors of the three constructs were different. To analyze how interactions via the Habc domain affect the motion of stx::pHGFP, we compared the behavior of the FL construct with that of the SNARE construct. The main effect of the Habc domain deletion was an increase in the frequency of short pauses (SNARE, 0.007 s^{-1}, vs FL, 0.002 s^{-1}; $p = 0.07$) (Fig. 4*D*). Extrasynaptic diffusion coefficients were hardly affected by this deletion (SNARE, 0.25, vs FL, 0.20 $\mu m^2/s$; $p < 10^{-4}$, KS test), and the distributions of synaptic diffusion coefficients for the SNARE and the FL constructs were not significantly different (Fig. 4*C*). The proportion of confined trajectories was unchanged, at both synaptic and extrasynaptic regions. Then, to address the contribution of interactions via the SNARE domain to the motion of stx::pHGFP, we compared the behavior of the SNARE construct (mainly composed of the SNARE and TMR domains) with that of

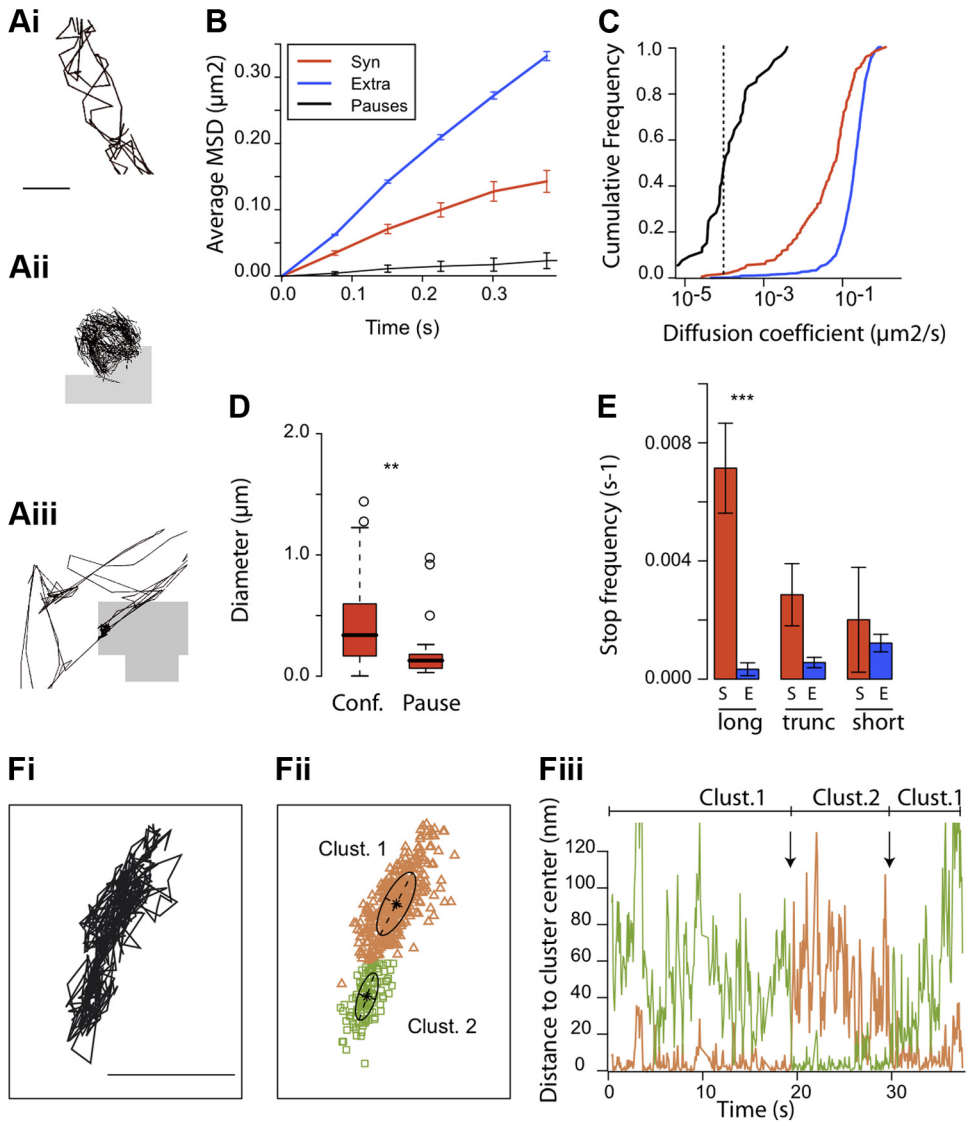

Figure 3. Lateral diffusion of stx::pHGFP coupled to QDs. ***A***, Examples of trajectories of stx::pHGFP coupled to QDs. The motion can be Brownian (***Ai***), confined (***Aii***), or display a pause (***Aiii*** and see text). The gray regions on ***Aii*** and ***Aiii*** correspond to synapses identified by FM4-64 labeling. Scale bar, 300 nm. ***B***, Average MSD (±SEM) for synaptic (red) and extrasynaptic (blue) trajectories, and for pauses (black). ***C***, Cumulative frequencies of the diffusion coefficients. The color code is the same as in ***B***. The vertical dotted line indicates the threshold for quantum dots considered immobile, as measured on blank coverslips. ***D***, Characteristic length of confinement at synapses (conf) and diameter of the area explored during pauses (median and 25–75% IQR, whiskers: 5 and 95% confidence limits). KS test, $^{**}p < 0.01$. ***E***, Frequencies (mean ± SEM) of the long, truncated (trunc), and short pauses, at synapses (red) or extrasynaptic regions (blue). Two-tailed Student's *t* test, $^{***}p < 0.001$. ***F***, Example of a "subcompartmental" trajectory. ***Fi***, Trajectory of a synaptic pause. Scale bar, 100 nm. ***Fii***, Two Gaussian clusters of positions were identified by a Gaussian mixture analysis (see Materials and Methods) and are shown here in orange and green. ***Fiii***, Distance of the QD to the center of each cluster (identified in ***Fii***) as a function of time (cluster 1, orange; cluster 2, green). At first, the distance of the QD to the center of cluster 1 is very small compared with that of cluster 2, indicating that QD diffuses within cluster 1. Then, the QD moves to cluster 2 (arrow), as shown by the short distance to cluster 2 relative to cluster 1. Finally, it moves back to cluster 1 (arrow).

the TMR construct (lacking the SNARE domain). In the absence of the SNARE domain, the frequency of short pauses at synapses was reduced from 0.007 s^{-1} for the SNARE construct to 0.001 s^{-1} for the TMR construct ($p = 0.02$) (Fig. 4*D*). The distribution of the diffusion coefficients was shifted toward higher values both at synaptic regions (SNARE, 0.06 $\mu m^2/s$, vs TMR, 0.13 $\mu m^2/s$; $p = 0.01$) and at extrasynaptic sites (SNARE, 0.25, vs TMR, 0.27 $\mu m^2/s$; $p < 10^{-4}$, KS test) (Fig. 3*C*). The proportion of confined trajectories remained unchanged. To summarize, removal of the Habc domain resulted in a higher frequency of short pauses, whereas further removal of the SNARE domain decreased the frequency of short pauses and increased the diffusion coefficient. However, the pauses were relatively rare, which rendered the estimation of their frequency for each construct imprecise. This is likely to be due to the undersampling that is inherent to the SPT approach. Therefore, FRAP experiments were performed in an attempt to overcome this limitation of the SPT technique.

Intracellular interactions affect the exchange dynamics of stx::pHGFP

In FRAP experiments, the rates of fluorescence recovery of the various constructs were slower at synaptic than at extrasynaptic regions (Fig. 4*E*,*F*), as quantified by the levels of recovery at specific time points and by the parameters of the biexponential fit. At synapses, removal of the Habc domain slowed down the fluorescence recovery: the recovered fractions were 35 vs 51% after 6 s for the SNARE and FL construct, respectively ($p < 10^{-4}$), then 56 versus 68% after 28 s ($p = 0.009$), and 75 and 84%

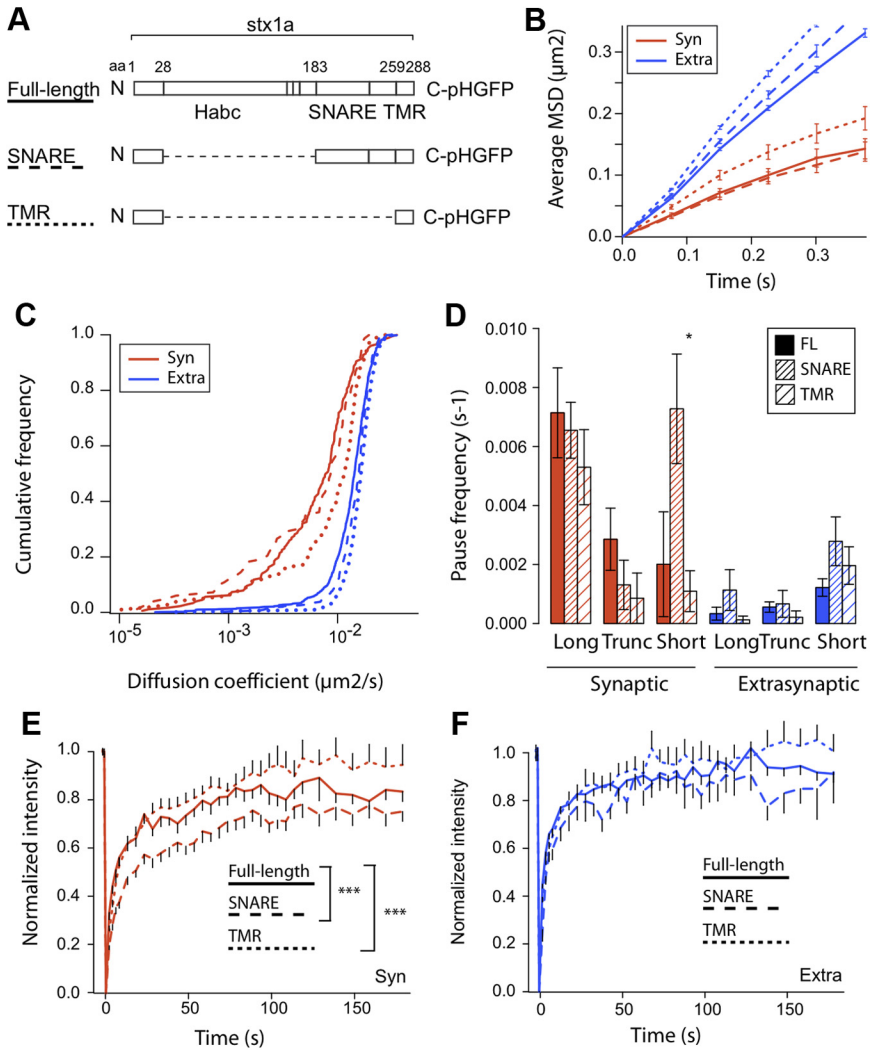

Figure 4. Effects of deletions of the Habc and SNARE domains on the lateral diffusion of stx::pHGFP. ***A***, Schematic representation of the three constructs of syntaxin. The full-length construct consists of syntaxin1a (stx1a) fused to the pHGFP at its C-terminal end. The Habc domain is deleted in the SNARE construct (amino acids 1–28, 183–288), and both the Habc and the SNARE domains are deleted in the TMR construct (amino acids 1–28, 259–288). ***B***, Average MSD (±SEM) for stx::pHGFP (solid lines), SNARE (dashed lines), and TMR (dotted lines) trajectories, at synaptic (red) or extrasynaptic (blue) regions. ***C***, Cumulative frequencies of the diffusion coefficients. The color code is the same as in ***B***. ***D***, Frequencies (mean ± SEM) of the long, truncated, and short pauses, at synapses or extrasynaptic regions, and for each construct (stx::pHGFP, filled; SNARE, tight hatches; TMR, loose hatches). ***E***, ***F***, Averaged normalized fluorescence recovery (mean ± SEM) of stx::pHGFP (solid line), the SNARE construct (dashed line), and the TMR construct (dotted line) versus time, at synaptic (***A***) and extrasynaptic (***B***). The stars indicate the maximum *p* value measured at a given time point on the curve (see text for details). Two-tailed *t* test, $*p < 0.05$, $*p < 0.001$.

at the plateau after 150 s ($p = 0.1$). Consistently, the biexponential fits indicated that the fraction P_f, corresponding to the short characteristic time, was smaller for the SNARE construct than for the FL construct (45 vs 55%; $p = 0.04$). Further removal of the SNARE domain led to a faster recovery. The levels of recovery for the TMR and the SNARE constructs were 46 versus 35% after 6 s ($p = 0.007$), 75 versus 56% after 28 s ($p = 0.0009$), and 95 versus 75% after 150 s ($p = 0.02$), respectively. Consistently, the short characteristic time τ_s of the biexponential fit was 143 s versus 261 s for the TMR and the SNARE constructs, respectively ($p = 0.05$), and the "fast fraction" P_f was, respectively, 60 versus 45% ($p = 0.006$). Finally, at extrasynaptic regions, the recovery was not significantly different between the three constructs, except for a slightly slower initial recovery for the SNARE construct compared with the FL construct. In conclusion, removal of the Habc domain of stx::pHGFP slowed down the fluorescence recovery process, and further removal of the SNARE domain accelerated the recovery. This was consistent with the differences in pause frequencies between the three constructs seen in SPT experiments (Fig. 4*D*).

Cleavage of the partner SNAP-25 affects the trajectories of stx::pHGFP

SNAP-25 is the other SNARE protein associated with the plasma membrane and involved in the SNARE complex. It is a palmitoylated protein, which forms a binary complex with syntaxin1A (Weninger et al., 2008). To study how the interaction between stx::pHGFP and SNAP-25 affects the motion of stx::pHGFP, we used the light chain of BoNT/E, which lyses the 26 C-terminal amino acid residues of SNAP-25, and thereby disrupts its interaction with syntaxin1A (Rickman et al., 2004). Because cleavage of SNAP-25 by BoNT/E blocks calcium-dependent evoked exocytosis (Washbourne et al., 2002; Sørensen et al., 2003), FM4-64 dye could no longer be used to label synapses. Therefore, experiments were performed in spinal cord cultured neurons from knock-in mice expressing the fusion protein gephyrin::mRFP (Calamai et al., 2009), gephyrin being a core component of the inhibitory postsynaptic differentiation (Fritschy et al., 2008) [inhibitory synapses represent ~65% of synapses in the spinal cord (Dumoulin et al., 1999)]. In these experiments, neurons from the gephyrin::mRFP knock-in mice were transfected with stx::pHGFP alone (control) or with stx::pHGFP together with the BoNT/E light chain. Stx::pHGFP expression was similar with and without BoNT/E: stx::pHGFP was regularly distributed along axons as in rat spinal cord neurons. In control neurons, the same diffusive behaviors as in rat neurons were observed (Fig. 5): at synapses compared with extrasynaptic regions, the diffusion coefficients were lower, the trajectories were more frequently confined (74.85 vs 43.90%; $p = 3 \times 10^{-5}$), the characteristic length of confinement was smaller (473 vs 710 nm; $p = 6 \times 10^{-4}$), and pauses were more frequent. In the presence of BoNT/E, synaptic and extrasynaptic behaviors remained different (smaller diffusion coefficient, higher proportion of confined trajectories and smaller confinement length, and more frequent pauses at synapses than at extrasynaptic regions). However, the cleavage of SNAP-25 by BoNT/E affected the diffusive behavior of stx::pHGFP compared with control conditions. The diffusion coefficient of stx::pHGFP was slightly increased at synaptic and extrasynaptic regions (0.12–0.13 $\mu m^2/s$, $p = 0.06$; and 0.18–0.23 $\mu m^2/s$, $p < 10^{-3}$, respectively) (Fig. 5*A*,*B*). The frequency of short synaptic pauses was not affected (Fig. 5*C*), but the frequency of all types of synaptic pauses taken together was decreased (0.032–0.017 s^{-1}; $p = 0.06$, Wilcoxon's test). Interestingly, the median duration of the synaptic pauses was decreased from 3.75 to 1.65 s during BoNT/E expression ($p = 0.11$, KS test). Finally, neither the fraction of confined trajectories nor the charac-

teristic length of confinement was changed. Overall, cleavage of SNAP-25 accelerated the diffusion of stx::pHGFP and tended to decrease the frequency and the duration of synaptic pauses.

Cleavage of the partner SNAP-25 affects the exchange dynamics of stx::pHGFP

FRAP was performed at synaptic and extrasynaptic regions, in neurons from the gephyrin::mRFP knock-in mice transfected with stx::pHGFP (control) alone or cotransfected with stx::pHGFP and BoNT/E. In control neurons as well as in cotransfected neurons, the recovery was slower at synaptic regions than at extrasynaptic regions (Fig. 5*D*). In the presence of BoNT/E, the extrasynaptic recovery rate was unchanged, but at synapses the recovery was faster than in control conditions (Fig. 5*D*). More specifically, the recovered fractions increased from 39 to 44% after 6 s (control conditions and BoNT/E, respectively; $p = 0.1$), then from 59 to 69% after 28 s ($p = 0.02$), and from 80 to 87% at 150 s ($p = 0.1$). The parameters of the biexponential fit were not significantly different, but a biexponential fit is not always appropriate for this type of recovery (Sprague et al., 2004, 2006).

Thus, preventing interaction between stx::pHGFP and SNAP-25 by using BoNT/E resulted in a faster recovery at synapses, which is consistent with SPT data. Since SNAP-25 interacts with the SNARE domain of stx::pHGFP, these results are also consistent with the increased mobility observed after removal of the SNARE domain of stx::pHGFP.

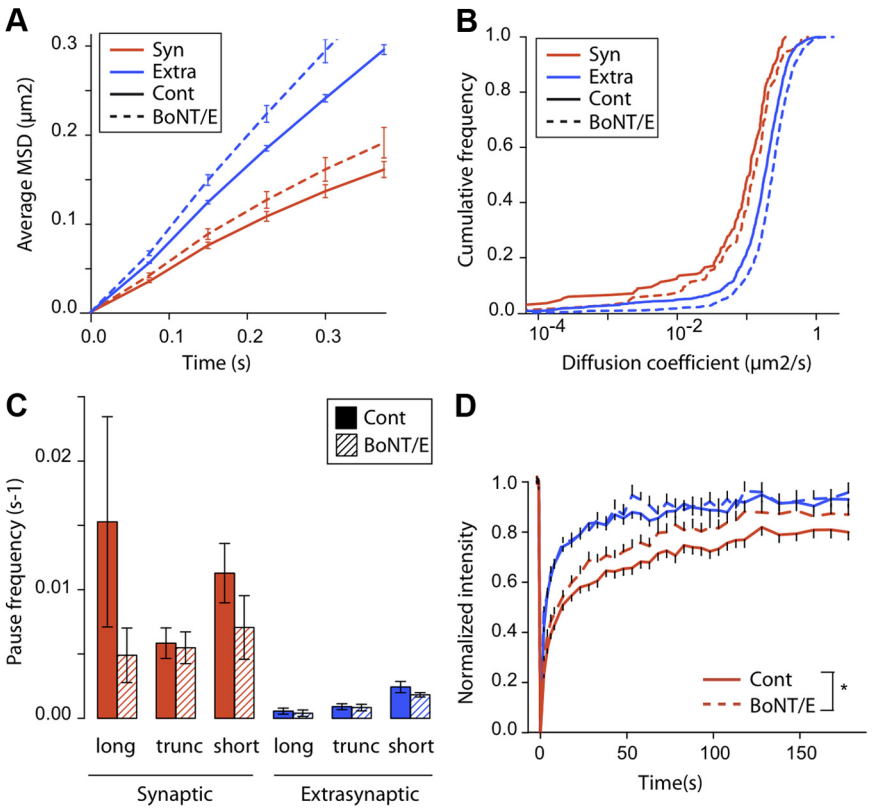

Figure 5. Effects of SNAP-25 cleavage on the lateral diffusion of stx::pHGFP. Neurons were transfected either with stx::pHGFP alone (control) or with both stx::pHGFP and the light chain of the BoNT/E, which specifically cleaves SNAP-25. ***A***, Average MSD (±SEM) of trajectories of stx::pHGFP in control (solid lines) and BoNT/E (dotted lines) conditions, at synaptic (red) or extrasynaptic (blue) regions. ***B***, Cumulative frequencies of the diffusion coefficients. The color and line codes are the same as in ***A***. ***C***, Frequencies (mean ± SEM) of the long, truncated, and short pauses, at synapses or extrasynaptic and for control (filled) and BoNT/E (hatches) conditions. ***D***, Averaged normalized fluorescence recovery (±SEM) of stx::pHGFP in control cells (solid line) and in cells cotransfected with BoNT/E (dotted line) versus time, at synaptic (red) and extrasynaptic (blue) locations. The star indicates the maximum *p* value measured at a given time point on the curve (see text for details). Two-tailed *t* test, $*p < 0.05$.

Dynamics of stx::pHGFP and synaptic activity

We also investigated the relationships between syntaxin diffusive motion and synaptic activity. On the one hand, the mobility characteristics of stx::pHGFP did not depend on the presence of calcium (no difference in FRAP recovery was observed with application of BAPTA) (Fig. 6) and were not significantly modified by tetrodotoxin (TTX) or 4-aminopyridin (4AP) bath applications (data not shown). On the other hand, impeding the mobility of stx::pHGFP by crosslinking using anti-GFP antibodies did not have any significant effect on the rate of exocytosis (FM unloading rate; data not shown). This absence of effect of neuronal activity on stx::pHGFP motion or conversely of stx::pHGFP reduced motion on synaptic activity may be due to technical limitations. First, the presence of endogenous syntaxin might hinder the effect of neuronal activity on stx::pHGFP motion or compensate for the effect of the reduced diffusion of crosslinked stx::pHGFP on exocytosis. Second, on application of TTX or BAPTA, exocytosis is not fully abolished, since miniature potentials still occur. Third, the timescale at which stx::pHGFP motion is affected by neuronal activity may be too small for the temporal resolution of our techniques (exocytosis occurs on the millisecond timescale). Finally, from a theoretical point of view, when the membrane of a vesicle—devoid of syntaxin (Mitchell and Ryan, 2004)—is integrated in the plasma membrane, the spatial organization of syntaxin is disrupted, and the time required to recover one-half of the initial concentration of stx::pHGFP at the site of exocytosis can be estimated as 0.002 s [based on the approach of Heine et al. (2008), with a diffusion coefficient 0.07 $\mu m^2/s$ and a 50 nm diameter for the area devoid of syntaxin]. Therefore, the rapid diffusion of syntaxin might allow the synaptic active zone to sustain high rates of exocytosis.

Additional kinetic parameters can be obtained by combining FRAP and SPT data within a model of diffusion and binding of stx::pHGFP

FRAP provides information about the "average" behavior of a population in a given region, but requires assumptions about the underlying diffusive properties of the individual molecules within their environment to further characterize the dynamic properties of molecules (Sprague et al., 2004, 2006). In contrast, SPT gives direct access to the diffusive motion of individual molecules but is limited by the intrinsic sampling of the method. To overcome these limitations, we have combined these methods within a biophysical model describing the diffusive behavior of stx::pHGFP, based on SPT data and the biological literature, which allows fitting of the experimental FRAP curves.

First, according to SPT experiments, the motion of stx::pHGFP alternates between diffusive periods and pauses, which can be short or long, and the characteristics of which depend on the SNARE domain of stx::pHGFP and SNAP-25 binding. This suggested, as developed in Discussion, that pauses reflect binding events related to

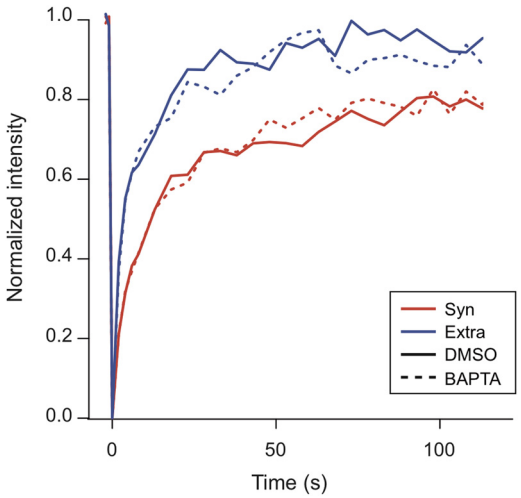

Figure 6. Absence of effect of calcium chelation with the membrane permeant agent BAPTA-AM on the FRAP recovery. Averaged normalized fluorescence recovery (±SEM) of stxGFP in control conditions with only DMSO (solid line) and in the presence of BAPTA (dotted line) versus time, at synaptic (red) and extrasynaptic (blue) locations.

the formation of the exocytotic complex. Second, the formation of the exocytotic complex is currently thought to proceed in two steps (Weninger et al., 2008): (1) the formation of an "acceptor complex," which involves syntaxin and SNAP-25; and (2) the transformation of this acceptor complex into the exocytotic complex, with the participation of synaptobrevin2, among others. Therefore, we propose the following three-state model to describe the diffusive behavior of stx::pHGFP:

(1) Stx::pHGFP in the free form, S_0, moves with Brownian motion;

(2) S_0 can be immobilized for a short period (seconds) by binding to a first partner M_1, thereby forming a complex S_1 ("acceptor complex");

(3) The immobilized acceptor complex S_1 can bind for a long period (minutes) to a second partner M_2, to form the complex S_2. In this description, the S_2 complex would correspond to the exocytotic complex.

This scenario is described by the following chemical reactions:

$$S_0 + M_1 \underset{k_{10}}{\overset{k_{01}}{=}} S_1$$

$$S_1 + M_2 \underset{k_{21}}{\overset{k_{12}}{=}} S_2,$$

where k_{01}, k_{12}, and k_{10}, k_{21} are the forward and backward binding rates for each reaction, respectively. The same model holds in the synaptic and extrasynaptic regions, but the values of the parameters may differ in each region, which is consistent with the experimental data (short and long pauses are observed in both regions) (see Discussion).

Diffusion coefficients of S_0 in each region were obtained from SPT as described above. Then, some reactions rates could also be estimated from SPT data. The backward rate of a binding reaction is the reciprocal of the mean binding duration (Schuss, 1980). For the first reaction, the parameter k_{10} could therefore be obtained directly from the duration of the short pauses measured in SPT. For the second reaction, the parameter k_{21} could not be precisely estimated from the SPT data because the long pauses were longer

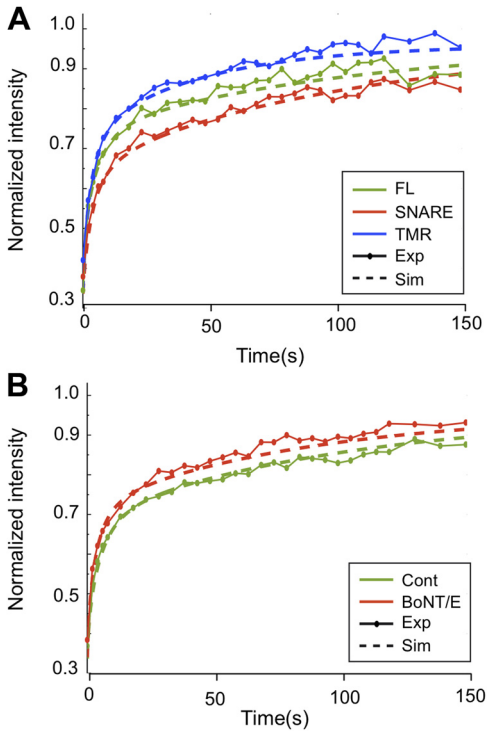

Figure 7. Simulations of FRAP with a model of two coupled binding reactions based on SPT data. ***A***, Simulation of FRAP for the three different constructs (stx::pHGFP, green; SNARE, red; TMR, blue) at synaptic regions. Experimental data are shown in solid line, and simulated data, in dashed line. ***B***, Simulation of FRAP for conditions with and without BoNT/E (control, green; BoNT/E, red) at synaptic regions. The line code is the same as in ***A***.

Table 1. Kinetic parameters of the modeled reactions in different experimental conditions

	FL		SNARE		TMR		Control		BoNT/E	
	Extra	Syn	Extra	Syn	Extra	Syn	Extra	Syn	Extra	Syn
k_{01} (s^{-1})	0, 08	0, 12	0, 70	1, 40	0, 60	1, 20	0, 16	0, 25	0, 16	0, 55
k_{10} (s^{-1})	**0, 22**	**0, 22**	**0, 80**	**0, 80**	**0, 83**	**0, 83**	**0, 40**	**0, 27**	**0, 40**	**0, 61**
k_{01}/k_{10}	0, 36	0, 54	0, 88	1, 75	0, 72	1, 44	0, 40	0, 94	0, 40	0, 91
k_{12} (s^{-1})	0, 01	0, 02	0, 01	0, 02	0, 02	0, 02	0, 01	0, 02	0, 01	0, 02
k_{21} (s^{-1})	0, 01	0, 01	0, 01	0, 01	0, 03	0, 020	0, 01	0, 01	0, 01	0, 01
k_{12}/k_{21}	0, 83	1, 60	0, 67	1, 60	0, 67	0, 80	0, 67	2, 13	0, 67	1, 42

Each column corresponds to a given experimental condition (FL,full-length stxGFP construct; SNARE, SNARE::pHGFP construct; TMR, TMR::pHGFP construct; control, control conditions in experiments with botulinum toxin; BoNT/E, experiments in presence of botulinum toxin) at extrasynaptic and synaptic locations. Parameters shown in bold are measured experimentally. Parameters in normal font are estimated from the fit of the FRAP curves. Rates are in seconds $^{-1}$.

than the recording time (37.5 s), but was expected to be on the order of minutes $^{-1}$. Finally, the forward rates k_{01} and k_{12} correspond to the frequency of the binding events. In principle, these frequencies can be measured in SPT experiments, but due to experimental limitations they could not be accessed with sufficient precision and were therefore left as free parameters in the model.

We first fitted extrasynaptic FRAP curves to derive a set of values for the extrasynaptic parameters. Then, to fit the synaptic curves (where recovery depends on the dynamics of syntaxin at both the synapse and the surrounding extrasynaptic region), the fitted values of the extrasynaptic parameters were used as inputs and only the synaptic parameters were adjusted (Fig. 7, Table 1). Although several sets of parameters could equally fit the experimental curves, the binding rates presented here (Table 1) are compatible with the experimental data (in particular, the back-

ward binding rate of the second reaction corresponds to a binding duration longer than the recording time). For all conditions, the affinity constants of both reactions (defined as the ratio of the forward to the backward binding rates, which is equal to the ratio of bound to free molecules at equilibrium) were higher at synaptic than extrasynaptic sites (roughly by a factor 2) (Table 1). This would correspond to a higher proportion of bound molecules at the synapse compared with the extrasynaptic region. The estimated fractions of syntaxin in states S_1, S_2, and S_0 were 40, 30, and 30% at synapses and 25, 15, and 60% at extrasynaptic regions, respectively. At synapses, deletion of the Habc domain increased the affinity constant of the first reaction, consistently with the increase in short pause frequency observed in SPT (Fig. 7*A*, Table 1). Further deletion of the SNARE domain led to a decrease of both synaptic affinity constants. We concluded that the SNARE domain was involved in both the short and long binding. Finally, cleavage of SNAP-25 resulted in a smaller affinity constant for the second reaction at synapses (Fig. 7*B*, Table 1). The long binding reaction was therefore "destabilized" in the absence of SNAP-25. Surprisingly, the affinity constant of the first reaction was unchanged, with a shorter duration of this short binding compensated for by a higher forward binding rate. Specific values of the forward and backward binding rates are considered in Discussion.

In conclusion, combining FRAP recovery modeling with SPT data allowed us to obtain a semiquantitative scenario and to extract parameters of the syntaxin dynamics: the diffusive behavior of syntaxin results from free diffusion and two coupled binding reactions, consistent with its involvement in the formation of the exocytotic complex.

Discussion

Using FRAP and SPT, we have characterized the diffusive behavior of stx::pHGFP, which reflects both free diffusion of the molecule and dynamic interactions with its partners. In addition, we have proposed a model that combines FRAP and SPT data and provides a semiquantitative characterization of these interactions. Below, we discuss how these interactions, which modulate the lateral mobility of stx::pHGFP, are related to the formation of the exocytotic complex, and how they lead to the transient stabilization of stx::pHGFP at the active zone.

Different diffusive behaviors of stx::pHGFP at synaptic and extrasynaptic regions

First, in FRAP experiments, the characteristic times of recovery at synaptic and extrasynaptic regions were particularly small: a few seconds, to be compared with many minutes for Munc13, a cytoplasmic protein accumulated in the presynaptic terminal (Kalla et al., 2006). Then, in SPT experiments, the diffusion coefficients were smaller at synaptic than at extrasynaptic regions, and the proportion of confined trajectories was higher—note that labeling of stx::pHGFP with a QD hardly limits its diffusion: the QD is present in the extracellular medium, and the motion of the QD-stx::pHGFP complex is first imposed by friction within the lipid membrane, which is 1000 times more viscous than the aqueous extracellular environment (Triller and Choquet, 2008; Alcor et al., 2009). The slowdown and confinement of stx::pHGFP at synapses can be due to fast interactions with obstacles or partners crowding the presynaptic active zone (Saxton, 1994, 1996; Deverall et al., 2005; Siksou et al., 2007), including membrane proteins such as calcium channels, adhesion proteins, and SNAP-25, as well as submembrane proteins such as Bassoon and Cast/Erc (Dresbach et al., 2001; Siksou et al., 2007). Furthermore, the characteristic length of confinement was ~330 nm, comparable with the diameter of the synaptic zone (400 nm) (Siksou et al., 2007). The fact that no difference in dwell time at synapses between confined trajectories and Brownian trajectories was detectable while a high proportion of trajectories were confined suggests that the difference in the dwell time is too small to be detected with our method, and therefore that confinement was not a major determinant of the recovery observed in FRAP experiments. Extrasynaptic confinement could also result from the presence of obstacles in the extrasynaptic plasma membrane (Kusumi et al., 1993).

A striking feature of stx::pHGFP diffusion was the occurrence of pauses, more frequently at synapses than at extrasynaptic regions. During pauses, the area explored by stx::pHGFP had a diameter of ~120 nm, a value comparable with the "caging diameter" of docked synaptic vesicles (100 nm) (Nofal et al., 2007; Westphal et al., 2008). The durations of pauses (seconds to minutes) were compatible with the duration of vesicle docking at the membrane (Lemke and Klingauf, 2005; Zhang et al., 2009). All these observations strongly suggest that pauses reflect interactions related to the formation of this exocytotic complex. In this respect, extrasynaptic pauses could correspond to loci for extrasynaptic exocytosis (Coggan et al., 2005) or could have occurred at unlabeled synapses: in rat neurons, only active synapses were labeled by the FM4-64 dye, and in neurons from mRFP::gephyrin-KI mice, excitatory synapses were not labeled [35% of the total number of synapses (Dumoulin et al., 1999)].

SNARE interactions reflected in the motion of stx::pHGFP

Perturbations of syntaxin interactions further supported the hypothesis. First, at synapses, the deletion of the Habc domain resulted in an increased frequency of short pauses, and a slower fluorescence recovery, compared with the full-length construct. The binding of Munc18 to the closed conformation of syntaxin1A via the Habc domain is known to inhibit binding of the SNARE domain of syntaxin1A to other molecules (Dulubova et al., 1999; Gerber et al., 2008). This suggests that the pauses and the slowdown of FRAP could be partly related to binding of stx::pHGFP via its SNARE domain. Indeed, further removal of the SNARE domain increased the diffusion coefficient at synapses, reduced the frequency of short pauses, and was associated with a faster fluorescence recovery in FRAP experiments. Partners that interact with the SNARE domain of syntaxin1A include SNAP-25 and synaptobrevin2 (Rizo and Südhof, 2002; Jahn and Scheller, 2006), synaptotagmin, complexin (Bowen et al., 2005), and tomosyn (Ashery et al., 2009), all of which are involved in the formation of the exocytotic complex. With SNAP-25 cleavage, the slight increase in the diffusion coefficient, the shorter duration of pauses, and the faster fluorescence recovery at synapses suggest a destabilization of the bound states of stx::pHGFP. The contribution of SNAP-25 to the pause behavior of stx::pHGFP further supports the hypothesis that the motion of stx::pHGFP reflects SNARE interactions related to the formation of the exocytotic complex. Actually, cleavage of SNAP-25 by BoNT/E may abolish SNAP-25 stx::pHGFP interaction only partially, since the N-terminal domain of SNAP-25 alone can bind to syntaxin (Weninger et al., 2008). However, the differences in stx::pHGFP diffusive behavior between control and BoNT/E conditions indicate that BoNT/E is functional. As a consequence, binding of the C-terminal domain of SNAP-25 to stx::pHGFP affects the diffusion of stx::pHGFP and likely the formation of the exocytosis complex. Finally, the TMR construct still exhibited few pauses. The transmembrane region is known to interact with itself to

form homodimers (Laage et al., 2000), and with calcium channels (Cohen et al., 2007). In addition, the exocytotic complex has already been described as a superassembly of SNARE complexes possibly involving other proteins such as calcium channels (Lu et al., 2008). Binding of the TMR construct to endogenous syntaxin1A or to calcium channels already immobilized within the exocytotic complex could account for short and long pauses. In summary, pauses are likely to correspond to binding events related to the formation of the exocytotic complex.

Toward a rational approach to combining FRAP and SPT in a model of diffusion and binding of stx::pHGFP

To characterize further the stx::pHGFP interactions, we propose a model for the dynamics of stx::pHGFP, resulting from switching between periods of diffusion and binding. Based on SPT observations, we propose that stx::pHGFP is involved in two coupled binding reactions, the first corresponding to short pauses (in seconds), and the second to long pauses (in minutes). When stx::pHGFP is not involved in these reactions, it diffuses freely (meaning either as a stx::pHGFP molecule or bound to cytoplasmic molecules such as Munc18, which do not hinder its diffusion). The experimental FRAP curves obtained in all the conditions mentioned above were fitted within this model. Estimated values of the affinity constants of the binding reactions were consistent with an inhibition of binding by Munc18, and with the involvement of the SNARE domain as well as SNAP-25 in these binding reactions. In all conditions, the forward rate of the first reaction estimated by fitting the experimental curves was higher than the frequency of short pauses measured in SPT. This underestimation of the experimental pause frequency could be accounted for by a sampling bias (e.g., limited access of the stx::pHGFP immobilized in superassemblies of SNARE complexes) or by an overestimation of the residence time at synapses. Finally, in a previous study in neuroendocrine cells, syntaxin diffusive behavior was described based only on free diffusion and homophilic interactions between syntaxin molecules forming clusters (Sieber et al., 2007). Our computational model is also compatible with the formation of clusters by proteins of the exocytotic complex, which could correspond to the binding partners M_1 and M_2. However, direct comparison between these results and the data presented here remains difficult, since the membrane organization and composition and the exocytosis mechanism differ between neuroendocrine cells and neurons. In summary, the computational model provided orders of magnitude for the kinetic parameters of stx::pHGFP interactions, although it may not capture all the complexity of syntaxin1A interactions. Importantly, this model shows that combination of population level (FRAP) and single molecule level (SPT) observations of the diffusive motion of a molecule allows characterization of the binding reactions reflected in the motion.

In conclusion, the lateral diffusion of stx::pHGFP was characterized by a fast diffusive motion, interrupted by periods associated with the formation of the exocytotic complex, which dramatically slows down the motion at precise locations. Further characterization of the specific interactions involved in the motion of syntaxin1A might help to confirm this scenario. It is also worth noting that full abolishment of the formation of the exocytotic complex may be hard to observe: for instance, neither the absence of SNAP-25 nor synaptobrevin2 prevents the occurrence of minis (Schoch et al., 2001; Washbourne et al., 2002). Finally, combination of FRAP and SPT data led to the identification of two different kinetics of interactions involved in the formation of the exocytotic complex. The combination of rapid diffusion with transient localized pauses alleviates the paradox of the structured but dynamic membrane.

References

Alcor D, Gouzer G, Triller A (2009) Single-particle tracking methods for the study of membrane receptors dynamics. Eur J Neurosci 30:987–997.

Ashery U, Bielopolski N, Barak B, Yizhar O (2009) Friends and foes in synaptic transmission: the role of tomosyn in vesicle priming. Trends Neurosci 32:275–282.

Bannai H, Lévi S, Schweizer C, Inoue T, Launey T, Racine V, Sibarita JB, Mikoshiba K, Triller A (2009) Activity-dependent tuning of inhibitory neurotransmission based on $GABA_AR$ diffusion dynamics. Neuron 62:670–682.

Bowen ME, Weninger K, Ernst J, Chu S, Brunger AT (2005) Single-molecule studies of synaptotagmin and complexin binding to the SNARE complex. Biophys J 89:690–702.

Calamai M, Specht CG, Heller J, Alcor D, Machado P, Vannier C, Triller A (2009) Gephyrin oligomerization controls GlyR mobility and synaptic clustering. J Neurosci 29:7639–7648.

Charrier C, Ehrensperger MV, Dahan M, Lévi S, Triller A (2006) Cytoskeleton regulation of glycine receptor number at synapses and diffusion in the plasma membrane. J Neurosci 26:8502–8511.

Choquet D, Triller A (2003) The role of receptor diffusion in the organization of the postsynaptic membrane. Nat Rev Neurosci 4:251–265.

Coggan JS, Bartol TM, Esquenazi E, Stiles JR, Lamont S, Martone ME, Berg DK, Ellisman MH, Sejnowski TJ (2005) Evidence for ectopic neurotransmission at a neuronal synapse. Science 309:446–451.

Cohen R, Marom M, Atlas D (2007) Depolarization-evoked secretion requires two vicinal transmembrane cysteines of syntaxin 1A. PLoS One 2:e1273.

Dahan M, Lévi S, Luccardini C, Rostaing P, Riveau B, Triller A (2003) Diffusion dynamics of glycine receptors revealed by single-quantum dot tracking. Science 302:442–445.

Deverall MA, Gindl E, Sinner EK, Besir H, Ruehe J, Saxton MJ, Naumann CA (2005) Membrane lateral mobility obstructed by polymer-tethered lipids studied at the single molecule level. Biophys J 88:1875–1886.

Dresbach T, Qualmann B, Kessels MM, Garner CC, Gundelfinger ED (2001) The presynaptic cytomatrix of brain synapses. Cell Mol Life Sci 58:94–116.

Dulubova I, Sugita S, Hill S, Hosaka M, Fernandez I, Südhof TC, Rizo J (1999) A conformational switch in syntaxin during exocytosis: role of munc18. EMBO J 18:4372–4382.

Dumoulin A, Rostaing P, Bedet C, Lévi S, Isambert MF, Henry JP, Triller A, Gasnier B (1999) Presence of the vesicular inhibitory amino acid transporter in GABAergic and glycinergic synaptic terminal boutons. J Cell Sci 112:811–823.

Dumoulin A, Lévi S, Riveau B, Gasnier B, Triller A (2000) Formation of mixed glycine and GABAergic synapses in cultured spinal cord neurons. Eur J Neurosci 12:3883–3892.

Edidin M, Zagyansky Y, Lardner TJ (1976) Measurement of membrane protein lateral diffusion in single cells. Science 191:466–468.

Ehrensperger MV (2007) Suivi de molécules uniques à l'aide de nanocristaux semiconducteurs: méthodes et application à l'étude de la dynamique du récepteur de la glycine. PhD thesis, Université Pierre et Marie Curie, Paris, France.

Fritschy JM, Harvey RJ, Schwarz G (2008) Gephyrin: where do we stand, where do we go? Trends Neurosci 31:257–264.

Garcia EP, McPherson PS, Chilcote TJ, Takei K, De Camilli P (1995) rbSec1A and B colocalize with syntaxin 1 and SNAP-25 throughout the axon, but are not in a stable complex with syntaxin. J Cell Biol 129: 105–120.

Gerber SH, Rah JC, Min SW, Liu X, de Wit H, Dulubova I, Meyer AC, Rizo J, Arancillo M, Hammer RE, Verhage M, Rosenmund C, Südhof TC (2008) Conformational switch of syntaxin-1 controls synaptic vesicle fusion. Science 321:1507–1510.

Gómez-Varela D, Kohl T, Schmidt M, Rubio ME, Kawabe H, Nehring RB, Schäfer S, Stühmer W, Pardo LA (2010) Characterization of Eag1 channel lateral mobility in rat hippocampal cultures by single-particle-tracking with quantum dots. PloS One 5:e8858.

Hagiwara A, Fukazawa Y, Deguchi-Tawarada M, Ohtsuka T, Shigemoto R (2005) Differential distribution of release-related proteins in the hip-

pocampal CA3 area as revealed by freeze-fracture replica labeling. J Comp Neurol 489:195–216.
Hanus C, Ehrensperger MV, Triller A (2006) Activity-dependent movements of postsynaptic scaffolds at inhibitory synapses. J Neurosci 26:4586–4595.
Heine M, Groc L, Frischknecht R, Béïque JC, Lounis B, Rumbaugh G, Huganir RL, Cognet L, Choquet D (2008) Surface mobility of postsynaptic AMPARs tunes synaptic transmission. Science 320:201–205.
Jahn R, Scheller RH (2006) SNAREs—engines for membrane fusion. Nat Rev Mol Cell Biol 7:631–643.
Kalla S, Stern M, Basu J, Varoqueaux F, Reim K, Rosenmund C, Ziv NE, Brose N (2006) Molecular dynamics of a presynaptic active zone protein studied in Munc13-1-enhanced yellow fluorescent protein knock-in mutant mice. J Neurosci 26:13054–13066.
Kusumi A, Sako Y, Yamamoto M (1993) Confined lateral diffusion of membrane receptors as studied by single particle tracking (nanovid microscopy). Effects of calcium-induced differentiation in cultured epithelial cells. Biophys J 65:2021–2040.
Laage R, Rohde J, Brosig B, Langosch D (2000) A conserved membrane-spanning amino acid motif drives homomeric and supports heteromeric assembly of presynaptic SNARE proteins. J Biol Chem 275:17481–17487.
Lemke EA, Klingauf J (2005) Single synaptic vesicle tracking in individual hippocampal boutons at rest and during synaptic activity. J Neurosci 25:11034–11044.
Lévi S, Schweizer C, Bannai H, Pascual O, Charrier C, Triller A (2008) Homeostatic regulation of synaptic GlyR numbers driven by lateral diffusion. Neuron 59:261–273.
Lippincott-Schwartz J, Snapp E, Kenworthy A (2001) Studying protein dynamics in living cells. Nat Rev Mol Cell Biol 2:444–456.
Lu X, Zhang Y, Shin YK (2008) Supramolecular SNARE assembly precedes hemifusion in SNARE-mediated membrane fusion. Nat Struct Mol Biol 15:700–706.
Martinez-Arca S, Alberts P, Zahraoui A, Louvard D, Galli T (2000) Role of tetanus neurotoxin insensitive vesicle-associated membrane protein (TI-VAMP) in vesicular transport mediating neurite outgrowth. J Cell Biol 149:889–900.
Misura KM, Scheller RH, Weis WI (2000) Three-dimensional structure of the neuronal-Sec1-syntaxin 1a complex. Nature 404:355–362.
Mitchell SJ, Ryan TA (2004) Syntaxin-1A is excluded from recycling synaptic vesicles at nerve terminals. J Neurosci 24:4884–4888.
Mitchell SJ, Ryan TA (2005) Munc18-dependent regulation of synaptic vesicle exocytosis by syntaxin-1A in hippocampal neurons. Neuropharmacology 48:372–380.
Nofal S, Becherer U, Hof D, Matti U, Rettig J (2007) Primed vesicles can be distinguished from docked vesicles by analyzing their mobility. J Neurosci 27:1386–1395.
Racine V, Sachse M, Salamero J, Fraisier V, Trubuil A, Sibarita JB (2007) Visualization and quantification of vesicle trafficking on a three-dimensional cytoskeleton network in living cells. J Microsc 225:214–228.
Rickman C, Meunier FA, Binz T, Davletov B (2004) High affinity interaction of syntaxin and SNAP-25 on the plasma membrane is abolished by botulinum toxin E. J Biol Chem 279:644–651.
Rizo J, Rosenmund C (2008) Synaptic vesicle fusion. Nat Struct Mol Biol 15:665–674.
Rizo J, Südhof TC (2002) Snares and munc18 in synaptic vesicle fusion. Nat Rev Neurosci 3:641–653.
Sankaranarayanan S, De Angelis D, Rothman JE, Ryan TA (2000) The use of pHluorins for optical measurements of presynaptic activity. Biophys J 79:2199–2208.
Saxton MJ (1994) Anomalous diffusion due to obstacles: a Monte Carlo study. Biophys J 66:394–401.
Saxton MJ (1996) Anomalous diffusion due to binding: a Monte Carlo study. Biophys J 70:1250–1262.
Saxton MJ, Jacobson K (1997) Single-particle tracking: applications to membrane dynamics. Annu Rev Biophys Biomol Struct 26:373–399.
Schoch S, Deák F, Königstorfer A, Mozhayeva M, Sara Y, Südhof TC, Kavalali ET (2001) SNARE function analyzed in Synaptobrevin/VAMP knockout mice. Science 294:1117–1122.
Schuss Z (1980) Theory and applications of stochastic differential equations. New York: Wiley.
Sieber JJ, Willig KI, Kutzner C, Gerding-Reimers C, Harke B, Donnert G, Rammner B, Eggeling C, Hell SW, Grubmüller H, Lang T (2007) Anatomy and dynamics of a supramolecular membrane protein cluster. Science 317:1072–1076.
Siksou L, Rostaing P, Lechaire JP, Boudier T, Ohtsuka T, Fejtová A, Kao HT, Greengard P, Gundelfinger ED, Triller A, Marty S (2007) Three-dimensional architecture of presynaptic terminal cytomatrix. J Neurosci 27:6868–6877.
Singer SJ, Nicolson GL (1972) The fluid mosaic model of the structure of cell membranes. Science 175:720–731.
Söllner T, Whiteheart SW, Brunner M, Erdjument-Bromage H, Geromanos S, Tempst P, Rothman JE (1993) SNAP receptors implicated in vesicle targeting and fusion. Nature 362:318–324.
Sørensen JB, Nagy G, Varoqueaux F, Nehring RB, Brose N, Wilson MC, Neher E (2003) Differential control of the releasable vesicle pools by SNAP-25 splice variants and SNAP-23. Cell 114:75–86.
Sprague BL, Pego RL, Stavreva DA, McNally JG (2004) Analysis of binding reactions by fluorescence recovery after photobleaching. Biophys J 86:3473–3495.
Sprague BL, Müller F, Pego RL, Bungay PM, Stavreva DA, McNally JG (2006) Analysis of binding at a single spatially localized cluster of binding sites by fluorescence recovery after photobleaching. Biophys J 91:1169–1191.
Star EN, Kwiatkowski DJ, Murthy VN (2002) Rapid turnover of actin in dendritic spines and its regulation by activity. Nat Neurosci 5:239–246.
Südhof TC (2004) The synaptic vesicle cycle. Annu Rev Neurosci 27:509–547.
Südhof TC, Rothman JE (2009) Membrane fusion: grappling with SNARE and SM proteins. Science 323:474–477.
Triller A, Choquet D (2008) New concepts in synaptic biology derived from single-molecule imaging. Neuron 59:359–374.
Tsuriel S, Geva R, Zamorano P, Dresbach T, Boeckers T, Gundelfinger ED, Garner CC, Ziv NE (2006) Local sharing as a predominant determinant of synaptic matrix molecular dynamics. PLoS Biol 4:e271.
Tsuriel S, Fisher A, Wittenmayer N, Dresbach T, Garner CC, Ziv NE (2009) Exchange and redistribution dynamics of the cytoskeleton of the active zone molecule Bassoon. J Neurosci 29:351–358.
Vereb G, Szöllosi J, Matkó J, Nagy P, Farkas T, Vigh L, Mátyus L, Waldmann TA, Damjanovich S (2003) Dynamic, yet structured: the cell membrane three decades after the Singer–Nicolson model. Proc Natl Acad Sci U S A 100:8053–8058.
Washbourne P, Thompson PM, Carta M, Costa ET, Mathews JR, Lopez-Benditó G, Molnár Z, Becher MW, Valenzuela CF, Partridge LD, Wilson MC (2002) Genetic ablation of the t-SNARE SNAP-25 distinguishes mechanisms of neuroexocytosis. Nat Neurosci 5:19–26.
Weninger K, Bowen ME, Choi UB, Chu S, Brunger AT (2008) Accessory proteins stabilize the acceptor complex for synaptobrevin, the 1:1 syntaxin/SNAP-25 complex. Structure 16:308–320.
Westphal V, Rizzoli SO, Lauterbach MA, Kamin D, Jahn R, Hell SW (2008) Video-rate far-field optical nanoscopy dissects synaptic vesicle movement. Science 320:246–249.
Wu MN, Fergestad T, Lloyd TE, He Y, Broadie K, Bellen HJ (1999) Syntaxin 1A interacts with multiple exocytic proteins to regulate neurotransmitter release in vivo. Neuron 23:593–605.
Zhang Q, Li Y, Tsien RW (2009) The dynamic control of kiss-and-run and vesicular reuse probed with single nanoparticles. Science 323:1448–1453.